Characterization and extraction of global positioning system multipath signals using an improved particle-filtering algorithm

2011 Meas. Sci. Technol. 22 075101

(http://iopscience.iop.org/0957-0233/22/7/075101)

Meas. Sci. Technol. **22** (2011) 075101 (11pp) doi:10.1088/0957-0233/22/7/075101

Characterization and extraction of global positioning system multipath signals using an improved particle-filtering algorithm

Ting-Hua Yi[1,2,3], **Hong-Nan Li**[1] **and Ming Gu**[2]

[1] Faculty of Infrastructure Engineering, State Key Laboratory of Structural Analysis for Industrial Equipment, Dalian University of Technology, Dalian 116023, People's Republic of China
[2] State Key Laboratory for Disaster Reduction in Civil Engineering, Tongji University, Shanghai 200092, People's Republic of China

E-mail: yth@dlut.edu.cn

Received 29 June 2010, in final form 14 April 2011
Published 20 May 2011
Online at stacks.iop.org/MST/22/075101

Abstract
Driving down multipath errors is probably the single most important objective of the current research into the use of the global positioning system (GPS) for high-accuracy applications. This paper focuses on the characterization of multipath signals and techniques for their removal by improved particle filtering. By the characteristic analysis of the GPS multipath signal in carrier phase observations, a specific set of generating and monitoring systems for multipath signals is established and a series of controlled experiments are carried out to assess the efficiency of the improved particle filtering. Experimental results show that the method has the advantage of being able to adapt to the close reflector situation, while remaining quite efficient when the reflector gets further away. The extracted multipath signals may be used to improve positioning accuracies.

Keywords: GPS, multipath effects, particle filtering

(Some figures in this article are in colour only in the electronic version)

1. Introduction

With the sophisticated Global Navigation Satellite System (GNSS), the static and kinematic deformations of the large-scale structures can be monitored in the real-time mode with three-dimensional positioning precision to several millimeters. The applications include bridge, dam, pipeline and machinery alignment monitoring. In such scenarios, it is advantageous if the coordinates of target points can be provided with high data rates and high accuracy. The global positioning system (GPS) is an attractive system for providing such data since it is weather independent, has high precision positioning and short observation time, is capable of autonomous operation and does not require a line of sight (LOS) between target points [1]. However, the GPS satellite signals are susceptible to many kinds of error sources, such as ionospheric and tropospheric errors, orbital errors, clock errors and multipath effects. A double-differencing technique is commonly used for constructing the functional model as it can eliminate or reduce many of the troublesome GPS biases. But two unmodeled biases still remain that have not been well eliminated even after data differencing by past research efforts. The first is the dilution of precision (DOP) error that results from suboptimally oriented satellites. This error is inherent in the technology and can only be practically remedied through the addition of more satellites. The other error source is the multipath effect that occurs when duplicate satellite transmissions are received by the GPS antenna: one coming along a direct path from the satellite and the other arriving at a slight delay after reflecting off a nearby surface. The result is a long-period distortion in the displacement measurements that has been shown to induce errors of up to several meters in pseudorange estimates [2]. Thus, the multipath has become a major residual error source in the double-differenced GPS observables and an effective multipath

[3] Author to whom any correspondence should be addressed.

error eliminating method should be explored to improve the positioning precision.

As is known, the multipath disturbance is largely dependent on the receiver's environment since satellite signals can arrive at the receiver via multiple paths due to reflections from nearby objects. The use of choke ring antennas and the careful selection of antenna site may effectively mitigate the multipath, but it cannot always work. For example, in dense urban areas, the improvements of position accuracy may be limited because the obstruction of signals by high buildings results in bad geometries and multipath effects. There are also some applications, such as volcano and open cut mine slope monitoring, for which it is often impossible to identify antenna sites which are not vulnerable to multipath. In the case of volcano monitoring, all the GPS receivers have to be placed on the slope or at the foot of the mountain. The only antenna site which may be free of multipath is the one on the summit, where there is often a great reluctance to install a receiver. Hence, it is necessary to investigate data post-processing techniques for mitigating multipath. Early in 2000, Peyret *et al* [3] pointed out that the raw GPS measurements are not accurate enough due to the bias error, or drift, which is correlated with the constellation plot, through some local phenomena such as multi-path effects. By the analysis of the typical RTK GPS set of data using Fourier transform, they extracted two different components: a high-frequency noise, rather easy to filter, and a low-frequency bias. A site experiment was carried out, and the experimental results showed that the extracted bias, given its good repeatability, can be modeled and used in prediction to improve in real-time the raw accuracy of the data. Satirapod *et al* [4] proposed a multipath mitigation technique based on the wavelet transform, but the method was affected by the determination of wavelet bases and wavelet decomposition levels. Wang *et al* [5] further expanded this work, and presented an EMD-wavelet systematic error mitigation model. To identify and eliminate multipath sources, Axelrad *et al* [6] suggested analyzing the signal-to-noise ratio (SNR) of GPS signals. Multipath reflectors are identified by isolating segments of the SNR data with strong spectral peaks. The shortcoming of the method is that it cannot be implemented in real time. Bétaille *et al* [7] designed an intelligent adaptive algorithm that could combine three multipath observables (phase multipath mitigation window, SNR and multipath code error). The method can improve the observation precision under static conditions; however, it has not been proved under dynamic conditions. Fan *et al* [8] developed commercial software plus modules based on an electromagnetic modeling technique to process the carrier phase multipath error parameters. Static multipath modeling experiments showed that it could reduce carrier phase errors about 35% and 3D positioning errors about 25%, but dynamic experiments were not performed to verify its validity. Rouabah *et al* [9] proposed a method based on the use of the virtual multipath mitigation (VMM) technique [10], which proved limited due to the finite-bandwidth filter in the receiver that created an offset between the peak location of the virtual and the actual LOS. Numerical simulation results showed that the multipath signals' delay and coefficient amplitudes could be estimated. Nagano *et al* [11] proposed a novel technique for converting a C/A code into a shorter code, which saved 98% of memory necessary for the multipath estimation while preserving accuracy in code delay estimation. The results of numerical simulation showed that the code delay estimation error was close to the Cramer–Rao lower bound. Zhang *et al* [12] proposed a multipath mitigation technique based on the pseudorandom noise code autocorrelation function. This technique relied on the detection of the partial autocorrelation function that was affected by multipath signals. A thorough review of multipath mitigation methodologies concerning GPS high-precision deformation monitoring in civil engineering can be found by Zhang *et al* [13]. Despite attempts as mentioned above to mitigate the effects of the GPS multipath, generally these have led to improvements in the accuracy of phase measurements only to a certain extent.

In order to effectively mitigate the effects of multipath, it is necessary to have a detailed understanding of the signal transmitted from the satellite, the reflection process, the antenna characteristics and the way in which the reflected and direct signals are processed within the receiver. Unlike usual techniques, improved particle filtering has a number of characteristics that make it attractive for navigation and civil engineering applications. It is nonparametric, can effectively deal with nonlinearities and non-Gaussian noises, and is relatively easy to implement. Therefore, this paper tries to focus on the characterization of multipath signals and techniques for their removal in this kind of new way. As discussed above, a lot of data processing techniques have been advanced for solving the multipath effect problem; however, it is difficult to compare the proposed method in this paper to all of the existing methods since different methods have different scope. The structure of the paper is as follows: the characteristic analysis of the GPS multipath signal in carrier phase observations is given in section 2. The third section derives an improved particle-filtering algorithm for the GPS multipath signal filtering. A specific set of generating and monitoring systems for the GPS multipath signals is established in section 4. Following that, a series of controlled experiments is carried out to assess the capabilities of the multipath mitigation strategy, and the discussion of the test results compared with the previous work is given in section 5. The last section summarizes the findings of the paper and offers a perspective on future work.

2. Model of multipath and its properties

2.1. Model of multipath propagation

As is well known, the multipath effects occur when the GPS signals arrive at a receiver site via multiple paths due to reflections from nearby objects, such as the ground and water surfaces, buildings, vehicles, hills and trees. The multipath distorts the C/A-code and P-code modulations, as well as the carrier phase observations [14]. As schematically represented in figure 1, the multipath can be due to reflecting surfaces in the environment of both the reception and the emission of the signals, since the satellite itself can create the multipath.

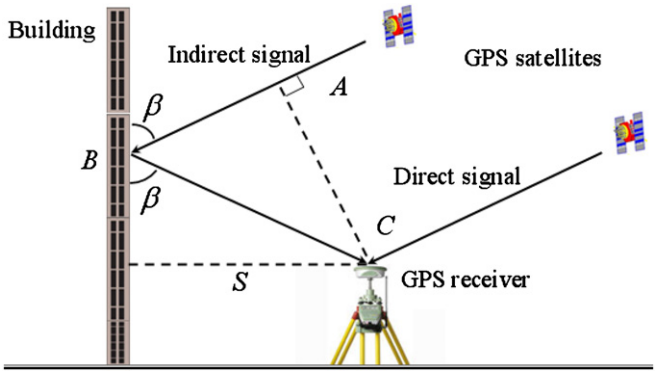

Figure 1. Multipath: geometry of a signal, a reflector and a receiver antenna.

Note that any reflection due to a satellite will have the same effect on a pair of receivers in a local network, and it has no consequence in differential positioning (it is canceled between the receivers in the network). Thus, the multipath that is satellite originating will not be considered here. This section introduces the basic mathematical models for the carrier phase GPS multipath. They are derived here for the benefit of readers unfamiliar with the basic formulae. One assumption for the model is that the multipath source is both a single reflector and a planar surface. In practice, this assumption is an exception rather than a rule.

The multipath signals are always delayed compared to the LOS signals because of the longer travel paths caused by reflections. From the geometrical relations shown in figure 1, the wave path difference Δ between indirect and direct signal lengths from the satellite antenna to the receiving antenna can be calculated as follows:

$$\Delta = AB + BC = BC \cdot \cos(180^\circ - 2\beta) + \frac{S}{\sin\beta}$$
$$= 2S \cdot \sin\beta - \frac{S}{\sin\beta} + \frac{S}{\sin\beta} = 2S \cdot \sin\beta \quad (1)$$

where β indicates the satellite signal incidence angle of the reflected point and S denotes the horizontal distance from the antenna to the reflecting surface.

The phase delay between the reflection signal and the direct signal (take radian as unit) can be expressed as follows:

$$\varphi = \frac{\Delta}{\lambda} \cdot 2\pi = \frac{4\pi S \cdot \sin\beta}{\lambda} \quad (2)$$

where λ is the carrier wavelength (L_1 or L_2 for the GPS).

The mathematical models of the direct signal and reflected signal are written respectively as

$$S_{\mathrm{LOS}} = A\sin(\omega_0 t) \quad (3)$$

and

$$S_M(t) = \sum_{i=1}^{M} \alpha_i A \sin(\omega_0 t + \varphi_i) \quad (4)$$

where S_{LOS} is the direct signal, $S_M(t)$ denotes the reflected signal, A indicates the amplitude of the direct signal, ω_0 stands for the angular frequency, and α_i and φ_i represent the reflection coefficient ($0 \leqslant \alpha_i \leqslant 1$) and the phase delay of the reflected signal i, respectively.

Thus, the superposed signal (i.e. the true received GPS signal) is

$$S_{\mathrm{Total}}(t) = A\sin(\omega_0 t) + \sum_{i=1}^{M} \alpha_i A \sin(\omega_0 t + \varphi_i). \quad (5)$$

After trigonometric transform, the superposed signal can be given by

$$S_{\mathrm{Total}}(t) = \alpha_c A \sin(\omega_0 t + \varphi_c) \quad (6)$$

where α_c and φ_c respectively represent the reflection coefficient of superposed signal and the phase delay of the superposed signal relative to the direct signal, which can be given by the following equations:

$$\alpha_c = \sqrt{1 + \sum_{i=1}^{M} \alpha_i \sin 2\varphi_i + \left(\sum_{i=1}^{M} \alpha_i \cos\varphi_i\right)^2 + \left(\sum_{i=1}^{M} \alpha_i \sin\varphi_i\right)^2} \quad (7)$$

$$\varphi_c = \arctan\left(\frac{\sum_{i=1}^{M} \alpha_i \sin\varphi_i}{1 + \sum_{i=1}^{M} \alpha_i \cos\varphi_i}\right). \quad (8)$$

Analyzing equations (2) and (8), one can see that the multipath is characterized by four parameters: the reflection coefficient α, the distance S of the reflector to the antenna phase center, the angle of incidence of the satellite signal β and the carrier wavelength λ.

2.2. *Properties of the multipath*

There are two basic carrier phase frequencies, L_1 (1575.42 MHz) and L_2 (1227.60 MHz). These frequencies can also be expressed as a wavelength, where the wavelength L_1 equals 19.0 cm and the wavelength L_2 equals 24.4 cm. Advanced processing techniques may use a linear combination of both frequencies, giving a signal wavelength larger or smaller than the L_1 or L_2 carrier phase. Assume that there is only one reflected signal, take the L_1 carrier signal as an example, suppose the horizontal distance $S = 1$, and the incidence angle $\beta = [0^\circ, 90^\circ] = [0, 0.5\pi]$ rad, the variation of the multipath phase error with incidence angle is simulated for the different reflection coefficients $\alpha = 0.0$, 0.25, 0.5, 0.75 and 1.0, as shown in figure 2. From the figure, it can be seen that the multipath signals gradually increase with the reflection coefficient. The maximum multipath phase error occurs when the phase delay of the reflected signal $\varphi_i = (2n-1)\pi$ ($n = 1, 2, \ldots$). Converting this phase shift to range equal to $\lambda/4$ or, with the wavelength L_1, 19.0 cm, a maximum change in the range of approximately 4.8 cm. It is well known that the reflection coefficient α is related to the properties of the material itself. When there are metal materials around the GPS antenna, it may cause the total reflection to the electromagnetic wave, while for non-metallic materials, the multipath effect is related to the dielectric constant; the bigger the dielectric constant, the bigger the reflection.

It can be seen from equation (2), besides the dielectric constant, that the multipath effect is also related to the distance from the reflector to the antenna phase center. The

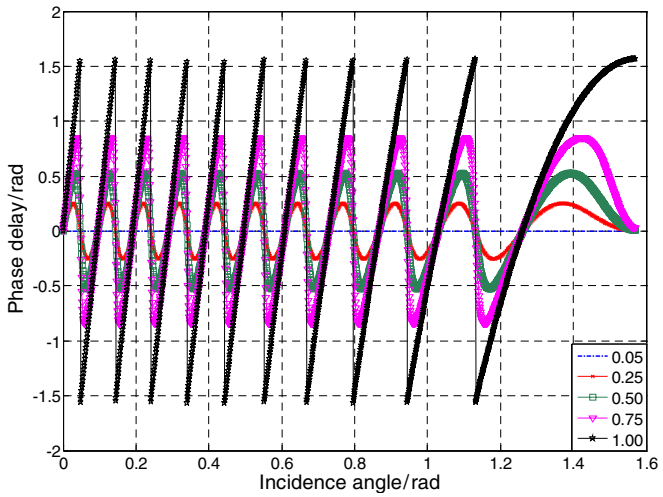

Figure 2. Multipath signals corresponding to different incidence angles ($S = 1$ m; $\alpha = 0.0$, 0.25, 0.5, 0.75 and 1.0).

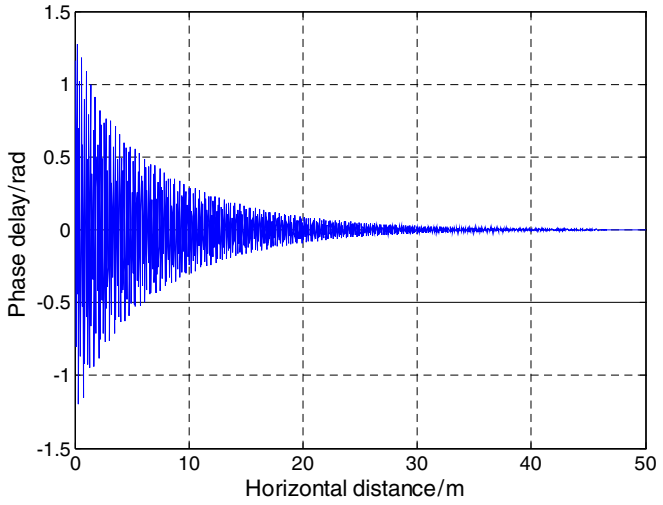

Figure 3. Multipath signals corresponding to different horizontal distances ($\beta = \pi/4$).

electromagnetic wave propagation equation in the atmosphere is mathematically given by [15]

$$I = I_0 \, \mathrm{e}^{-D\gamma} \tag{9}$$

where I_0 denotes the energy of the incident electromagnetic wave, I indicates the energy of the reflected electromagnetic wave, D stands for the wave propagation distance and γ represents the attenuation coefficient.

Suppose that the attenuation of the reflection coefficient obeys the electromagnetic wave transmission equation (9); letting $\beta = \pi/4$ as an example, the relationship between the multipath signals and reflecting distance can be simulated by equation (8). As is known, when the distance changes from 0 to 50 m, the energy of the reflected signal will attenuate to about 100 dB, and hence it can be ignored. It can be seen from figure 3 that the multipath phase error can also be ignored when the horizontal distance is more than 50 m.

The above discussion shows that highly reflective surfaces (to GPS signals) will lead to strong multipath signals (i.e. large amplitude), and objects close to the antenna will cause multipath signals with long wavelengths (conversely, distant objects usually cause multipath signals with short wavelengths). The key geometrical factor is the satellite elevation angle, with most reflected signals coming from nearby structures or the ground for a large incidence angle. The multipath is also a function of the carrier wavelength λ. Most of these factors are closely related to the reflecting environment.

3. Improved particle-filtering algorithm and its performance evaluation

3.1. Particle-filtering algorithm

From the above discussions, it can be concluded that the multipath effects cannot be easily mitigated. Fortunately, the multipath disturbance has a periodic characteristic and is repeated every sidereal day for a receiver if the antenna environment remains the same. The day-to-day repeatability of the multipath can be exploited to improve positioning accuracies. Therefore, it is necessary to accurately extract the multipath signals. However, the receiver's noise and multipath signal are mixed in the receiver. Hence, the receiver's noise should be properly and effectively eliminated first. Here, a particle-filtering algorithm is introduced to eliminate the receiver's noise [16].

The particle-filtering algorithm is a technique for implementing a recursive Bayesian filter by Monte Carlo simulations [17]. The key idea is to represent the required posterior density function by a set of random samples, which can be called particles with associated weights, and to compute estimates based on these samples and weights. Then the initial probability density distribution is updated by adjusting the weight and position of the particle. As the number of particles becomes very large, this Monte Carlo characterization becomes an equivalent representation to the usual functional description of the posterior probability density function (PDF), and the particle filtering approaches the optimal Bayesian estimate.

In order to develop the details of the algorithm, let $x = \{x^{(i)}, \omega^{(i)}\}_{i=1}^{n}$ denote a random measure that characterizes the posterior PDF $p(x_{0:k}|y_{1:k})$, where $\{x^{(i)}, i = 0, 1, \ldots, n\}$ is a set of support points with associated weights $\{\omega^{(i)}, i = 0, 1, \ldots, n\}$ and $x_{0:k} = \{x_j, j = 0, 1, \ldots, k\}$ is the set of all states up to the time k. The weights are normalized such that $\sum_i \omega_k^{(i)} = 1$. Then the posterior density at k can be approximated as

$$p(x_{0:k}|y_{1:k}) \approx \sum_{i=1}^{N} \omega_k^{(i)} \delta\left(x_{0:k} - x_{0:k}^{(i)}\right) \tag{10}$$

where $\delta\left(x_{0:k} - x_{0:k}^{(i)}\right)$ is the Dirac impulse function.

The weights can be chosen using the principle of importance sampling. If the importance density is chosen as

$$q\left(x_{0:k}|\, y_{1:k}\right) = q\left(x_k|x_{0:k-1}, y_{1:k}\right) q\left(x_{0:k-1}|\, y_{1:k-1}\right), \tag{11}$$

then after derivation, the weight update equation can be presented as

$$\omega_k^{*(i)} = \omega_{k-1}^{*(i)} \frac{p\left(y_k \left| x_k^{(i)}\right.\right) p\left(x_k^{(i)} \left| x_{k-1}^{(i)}\right.\right)}{q\left(x_k^{(i)} \left| x_{0:k-1}^{(i)}, y_{1:k}\right.\right)}. \tag{12}$$

Therefore, the basic steps of the particle-filtering algorithm can be drawn as follows.

(i) *Initialization*. Draw the particles $\left\{x_0^{(i)}\right\}_{i=1}^n$ from the prior density $p\,(x_0)$; the weights are normalized as $\sum_i \omega_k^{(i)} = 1$.

(ii) *Importance sampling*. Draw the particles $\left\{x_k^{(i)}\right\}_{i=1}^n$ from the importance density function $q\,(x_k | x_{0:k-1}, y_{1:k})$.

(iii) Evaluate the importance weights up to a normalizing constant: $\omega_k^{*(i)} = \omega_{k-1}^{*(i)} \frac{p(y_k|x_k^{(i)}) p(x_k^{(i)}|x_{k-1}^{(i)})}{q(x_k^{(i)}|x_{0:k-1}^{(i)}, y_{1:k})}$.

(iv) Normalize the importance weights: $\omega_k^{\sim(i)} = \frac{\omega_k^{*(i)}}{\sum_{i=1}^n \omega_k^{*(i)}}$.

The particle-filtering algorithm consists of the recursive propagation of the weights and support points as each measurement is received sequentially. It can be shown that as $n \to \infty$,, the result approaches the true posterior density.

3.2. Improved particle-filtering algorithm

The early form of the particle-filtering algorithm did not include resampling. A common problem with the method was the degeneracy phenomenon, where after a few iterations, all but one particle would have negligible weight. It has been shown that the variance of the importance weights can only increase over time, and thus, it is impossible to avoid the degeneracy phenomenon. This degeneracy implies that a large computational effort is devoted to updating particles whose contribution to the approximation is almost zero. The degeneracy phenomenon seriously limited the development of the particle filter. In 1993, Gordon proposed the sequential importance resampling (SIR) algorithm, and the problem was preliminarily solved [18]. Since then, quite a few different resampling-based particle-filtering algorithms have been found in the literature.

The idea of the resampling method is to eliminate the particles which have small normalized importance weights and concentrate upon particles with large weights. The resampling principle is that the posterior PDF $p\,(x_k |\, y_{1:k}) \approx \sum_{i=1}^{N_s} \omega_k^i \delta\left(x_k - x_k^i\right)$ is resampled N_s times to obtain the new support point $\left(x_k^{i*}\right)_{i=1}^{N_s}$, and then make $p\left(x_k^{i*} = x_k^i\right) = \omega_k^i$. Since the resampling is the independent and identical distribution, the weight is reset as $\omega_k^i = 1/N_s$. Generally, resampling is considered to be used only when the degeneracy phenomenon is below a fixed threshold, i.e. assume that the threshold is N_{th}. When the effective sample size $N_{\text{eff}} < N_{\text{th}}$, resampling should be used; otherwise it should not be used.

The most frequently encountered algorithms are multinomial resampling, stratified resampling, residual resampling and systematic resampling. The previous theoretical analyses [19, 20] showed that considering the resampling quality and computational complexity, systematic resampling is favorable over other resampling. The systematic resampling algorithm is generated based on the improvement of the multinomial resampling algorithm. It takes the algorithm one step further by deterministically linking all the variables drawn in the sub-intervals and turning the unordered random numbers into ordered. Additionally, from a uniform distribution perspective, systematic resampling is theoretically superior. Therefore, in this paper the systematic resampling algorithm is used. Suppose that $\{\xi^i, \omega^i\}_{1 \leqslant i \leqslant m}$ and $\{\tilde{\xi}^i, \tilde{\omega}^i\}_{1 \leqslant i \leqslant m}$ are the particle distributions before and after resampling, respectively, where ξ^i and $\tilde{\xi}^i$ are the ith particles, ω^i and $\tilde{\omega}^i$ present the corresponding weights, and m denotes the size of sampling. The steps are given as follows.

(i) Divide (0,1] into n intervals which are continuous but not overlapping, i.e. $(0,\,1] = (0,\,1/n) \cup \cdots \cup (\{n-1\}/n,\,1]$.

(ii) Obtain the sample set $U^i = i - 1/n + U$ by independent identical distribution sampling of each subinterval, where U is a single random drawn from $U((0,\,1/n])$.

(iii) Set $I^i = D_\omega^{\text{inv}}(U^i)$ and $\tilde{\xi}^i = \xi^{I^i}$, for $i = 1, \ldots, n$, where D_ω^{inv} is the inverse of the cumulative distribution function associated with the weight $\{\omega^i\}_{1 \leqslant i \leqslant m}$, that is, $D_\omega^{\text{inv}}(u) = i$, for $u \in \left(\sum_{j=1}^{i-1} \omega^j, \sum_{j=1}^{i} \omega^j\right]$. When needed, it can be denoted by $\xi |\, \{1, \ldots, m\} \to X$, the function such that $\xi(i) = \xi^i$, so that $\tilde{\xi}^i$ may also be written as $\xi \circ D_\omega^{\text{inv}}(U^i)$.

(iv) Set $\tilde{\omega}^i = 1/n, \quad \text{for} \quad i, \ldots, n$.

3.3. Numerical simulation

Numerical simulation studies are first carried out in order to demonstrate the feasibility of such filter schemes on the multipath signals, and to explore some of the characteristics of the improved particle filter.

Suppose the simulated data model is

$$y_t = x_t + e_t \tag{13}$$

where y_t denotes the multipath signal mixed receiver noise, x_t implies the simulated multipath signal sequence and e_t stands for the Gaussian white noise, which is assumed to be $e_t \sim N(0,\,2^2)$ with the unit of centimeter.

Suppose $x_t = 2\sin(0.05\pi t)$; the sampling interval of the simulated data is 0.1s and the sampling time is 400 s. Systematic resampling is selected as a resampling algorithm. As known, the derivative of the curve at one point is equal to the slope of the tangent line at the point. Thus, the system equation can be derived in the following expressions:

$$\begin{aligned} x_k - x_{k-1} &= \Delta t \cdot [2\sin(0.05\pi t)]' \\ &= 0.1 \cdot 0.1\pi \cos[0.05\pi(k-1)] = 0.01\pi \cos[0.05\pi(k-1)] \end{aligned} \tag{14}$$

where Δt denotes the sampling interval.

Suppose that the process noise w_k obeys the Gaussian distribution, i.e. $w_k \sim N(0,\,0.001^2)$; thus, the system equation can be given as

$$x_k = x_{k-1} + 0.01\pi \cos\left[0.05\pi\,(k-1)\right] + w_k. \tag{15}$$

The observation equation is given as

$$y_k = x_k + v_k \tag{16}$$

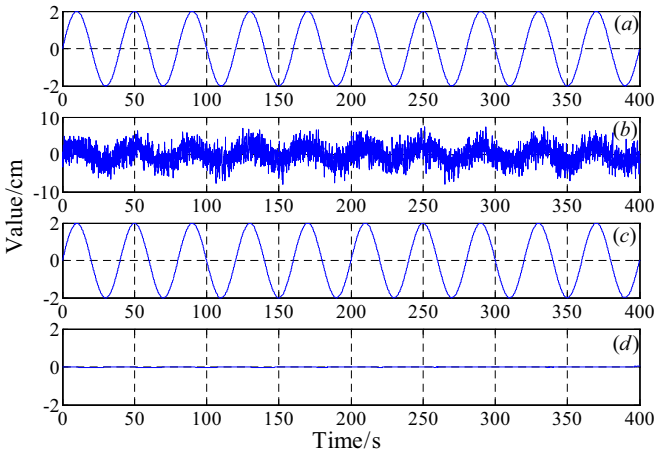

Figure 4. The filtering results of simulated data: (*a*) simulated multipath signal, (*b*) the mixed time series, (*c*) extracted multipath signal, (*d*) difference between the extracted and simulated multipath signal.

where the state x_k is the simulated multipath signal sequence and the observation value y_k denotes the multipath signal mixed receiver noise. The observation noise v_k is the supposed Gaussian white noise e_t, i.e. $v_k \sim N(0, 2^2)$. It is assumed that the posterior PDF obey the Gaussian distribution $p(x_0) \sim N(0, 0.001^2)$. First draw $N = 1000$ initial samples from $p(x_0)$ to obtain the particles. The importance density function is selected as $p(x_k|x_{k-1})$, and the resampling threshold value is $N_{\text{th}} = N/3$. The filtering results are shown in figure 4. To better quantify the filtering effect, the standard deviations and correlation coefficients are calculated. Note that after filtering, the standard deviation of the extracted multipath signal is 1.42, which indicates that the white noise has been indeed successfully reduced compared to the mixed time series 2.44. Similarly, the correlation coefficient between the extracted and simulated multipath signal is almost 1.0, which means that the improved particle-filtering algorithm can effectively eliminate the Gaussian white noise mixed in the simulated multipath signal by establishing the system equation and observation equation so long as the noise distribution is known.

4. Testing the system set-up

In order to rigorously assess the effectiveness of the method and investigate the characteristics of multipath signals, it is necessary to establish a well-defined testing methodology. For that, a specific system for GPS multipath signal generation and monitoring is established on the roof of the first laboratory building at the Dalian University of Technology, Dalian, China.

4.1. GPS monitoring system

A complete GPS monitoring system is mainly made up of three parts: data acquisition, data transmission and data processing and management. In this test, the reference site featured a high-precision Leica GRX1200 Pro GPS receiver and an AX1202 pinwheel antenna, which is susceptible to multipath signals with low-elevation trajectories, was placed on concrete pillars which were about 1.50 m in height. The rover site was equipped with a Leica GMX902 GPS receiver and the same pinwheel antenna used in full scale. Figure 5 illustrates the configuration of the GPS monitoring system.

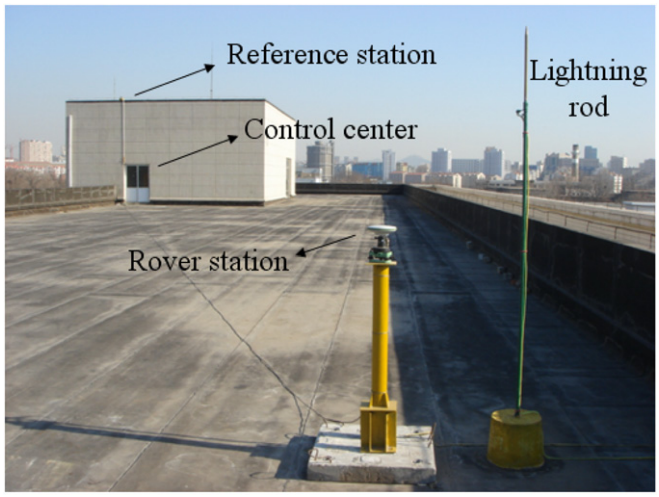

Figure 5. Configuration of the GPS monitoring system.

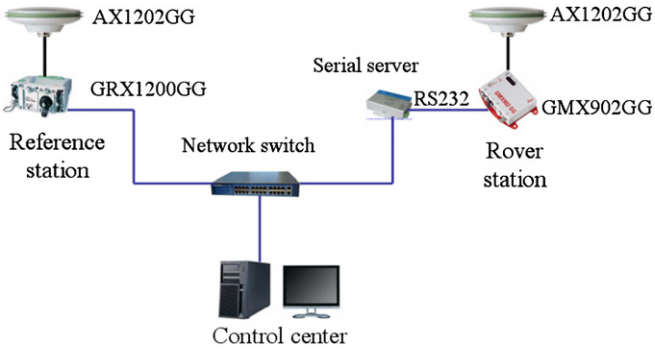

Figure 6. Composition of the GPS monitoring system.

The data transmission mode used is the network transmission, which is much more stable than the wireless transmission. The reference station, the rover station and the control center (data processing and management system) compose a local area network through the network switch, as shown in figure 6. The signals received by the reference station can be transmitted through the network directly, while the signals obtained by the rover station must be transmitted through the RS232 protocol; thus, a serial port server is needed to transform the RS232 protocol signals into the TCP/IP protocol network signals.

The data processing and management system (control center) includes a computer which is installed with the corresponding control software, the data processing, the analytical software and so on. The control software is the Leica GNSS Spider software, which can control the receivers as well as monitor the whole network. The Leica GNSS QC software was used to check the multipath effect and cycle slips on all the satellites tracked. For the data analysis, the codes were written using the MATLAB environment.

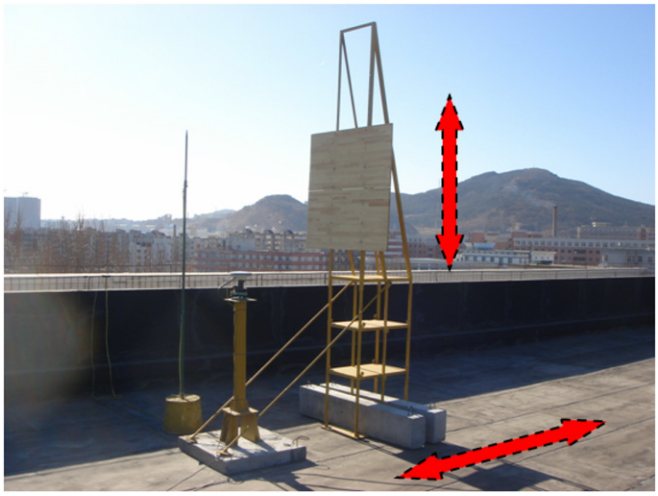

Figure 7. Set-up of the reflector near the rover antenna.

The baseline length between the two receivers is about 55 m. These units, when in a differential GPS configuration, can provide accuracy comparable to the aforementioned full-scale system, with fully real-time capabilities; since the top of the first laboratory building has excellent satellite visibility and minimal multipath sources, almost all GPS errors but receiver noise were eliminated.

4.2. Multipath signal generating system

For the purpose of generating the multipath in a controlled manner, an experimental set-up was designed that included a reflector (a 1.0 m × 1.0 m panel) and a steel frame brace, shown in figure 7. This can be used to generate the multipath with different characteristics depending on the distance between it and the rover station. Also, the height of the panel can be adjusted up or down.

5. Experimental studies of GPS multipath signals

5.1. Data acquisition processing

In the process of the experiment, the minimum satellite elevation angle was 10° and the sampling frequency was 10 Hz. Here, the hypothesis will always be made that there is no significant multipath at the rover station. The most important multipath will actually be due to the reflector.

The test includes the following four parts.

(1) In order to determine the 3D coordinates of the rover, a 1 day long GPS static observation was made.
(2) In order to investigate the noise characteristics of the receiver, 3 day long continuous kinematic GPS data collection was carried out with the antenna completely unobstructed to ensure that the receiver was not recording signals from any other source.
(3) In order to verify the effectiveness of the particle filtering on extracting the multipath signals from the real observation data, 2 day long continuous kinematic GPS data collection was carried out by setting aside the reflector near the rover's antenna. Additionally, the data were also logged for the transition period between no material and insertion of a material in front of the antenna, so as to confirm that the rover did not lose lock during the test.
(4) For the purpose of studying the characteristics of the multipath signals caused by the reflector at different distances, the reflector was placed on consecutive days at 1, 4 and 7 m from the antenna, on the antenna's west side (so that the reflector was facing east), in kinematic mode. The heights of the reflector at different distances were obtained according to the receiver's minimum satellite elevation angle (10°), as shown in figure 8.

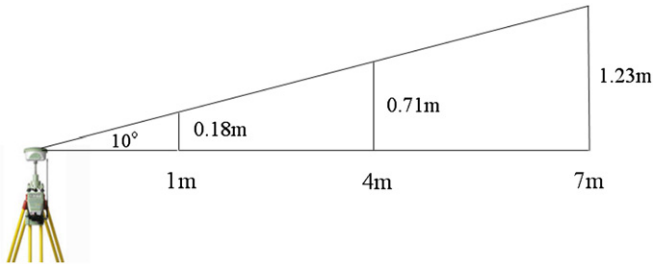

Figure 8. Heights of the reflector at different distances from the rover's antenna.

Table 1. Statistics of the GPS receiver's noise (unit: cm).

	Mean value			Standard deviation		
Days	N–S	W–E	Height	N–S	W–E	Height
First day	0.01	−0.16	0.03	0.26	0.27	0.39
Second day	−0.24	−0.06	0.29	0.25	0.21	0.52
Third day	−0.10	0.14	0.13	0.25	0.21	0.47

5.2. Study on the distribution of rover' noise

As discussed above, in the process of particle filtering, the selection of the state vector's initial values is not very important. Along with the iteration of filtering, the state vector will gradually converge to better values. Therefore, the proper selection of the observation noisy parameter is essential for the state estimation. In process (2) of the experiment, the 3 day long continuous kinematic GPS data were collected with the antenna completely unobstructed within 50 m. So the double-differenced carrier-phase residuals obtained from the receiver exhibit only 3D coordinates and observation noise. By subtracting the coordinates obtained in process (1) from the results of process (2), the receiver's system noises in the north–south, west–east and vertical directions can be obtained. The corresponding 1 h observation noises in three consecutive days are shown in figure 9. Table 1 summarizes the basic results calculated in three consecutive days as those of the receiver's noise.

From figure 9 and table 1, it can be seen that the consecutive 3 day long receiver's noise has no obvious relevance in 3D directions, and the amplitude variation range

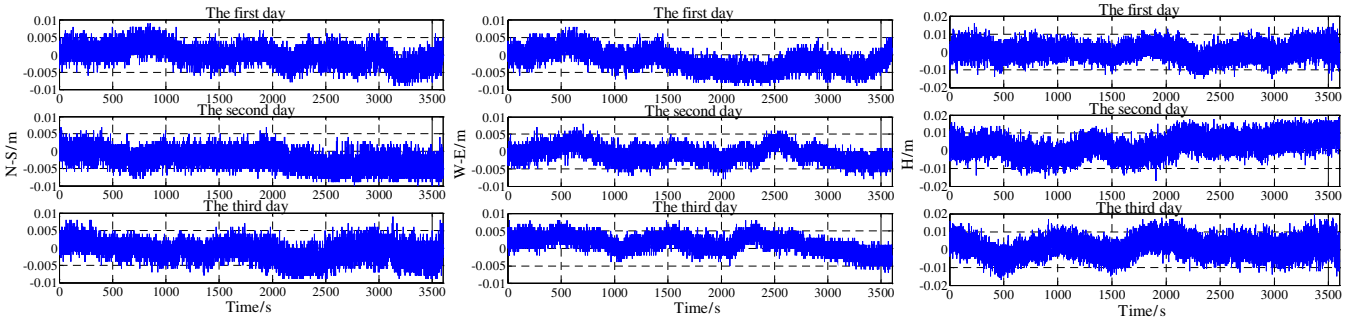

(*a*) N-S direction (*b*) W-E direction (*c*) Vertical direction

Figure 9. Receiver's noise series in 3D directions on three consecutive days.

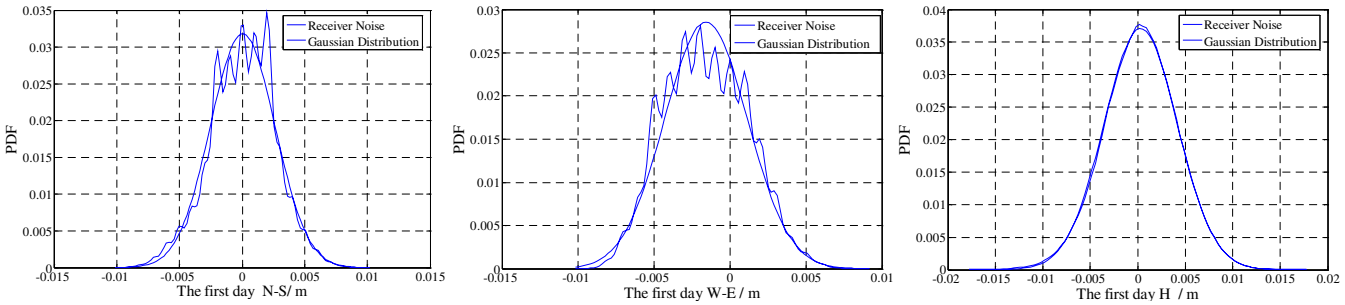

(*a*) N-S direction (*b*) W-E direction (*c*) Vertical direction

Figure 10. PDF of the receiver's noise on the first day in 3D directions.

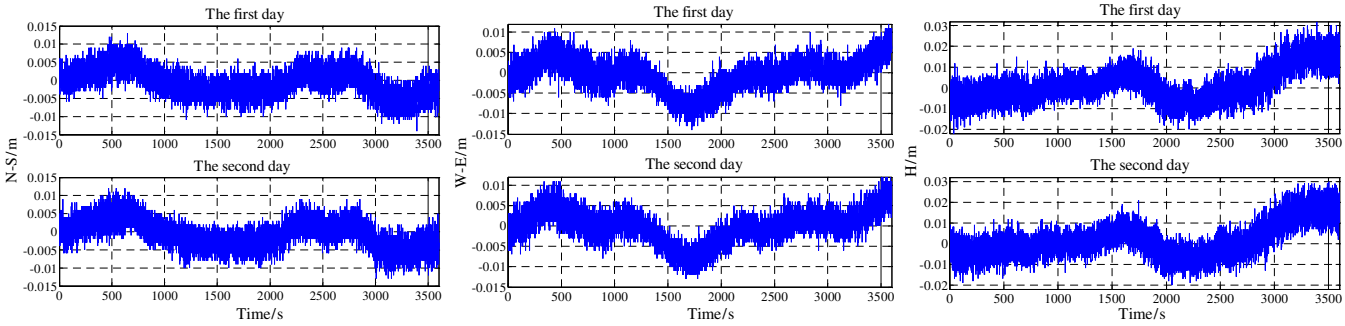

(*a*) N-S direction (*b*) W-E direction (*c*) Vertical direction

Figure 11. Observation results on two consecutive days in three directions.

is within the nominal accuracy of the receiver. To determine the distribution of the receiver's noise, the PDF of the receiver's noise are compared with its corresponding Gaussian distribution in each direction (the mean value and standard deviation of the Gaussian distribution are the same as those of noise), and it is found that the distributions of the receiver's noise match well with the Gaussian distribution, as shown in figure 10 (only the data of the first day are typically given here). This implies that the assumption of the Gaussian distribution is reasonable from the discussions herein. Based on the understanding of the receiver's noise as discussed here, we have reason to believe that the multipath signals could be extracted from the measurement data by the particle-filtering algorithm.

5.3. Filtered results for field measurement data

Since differential GPS positioning is used in the experiment, the public errors can be eliminated between the reference station and the rover station. The results of process (3) were only influenced by the multipath signals and receiver's system noise. Thus, the different values between the results of process (3) and process (2) are the mixed sequence of multipath signals and receiver's noise. Take 1 h data from two consecutive days (the time sequence of the second day is 3 min and 56 s ahead of the first day), as shown in figure 11; it can be seen that as the geometry between the GPS satellites and a specific receiver–reflector location repeats every sidereal day, the multipath tends to exhibit the same pattern on consecutive days. Although they look very similar, there

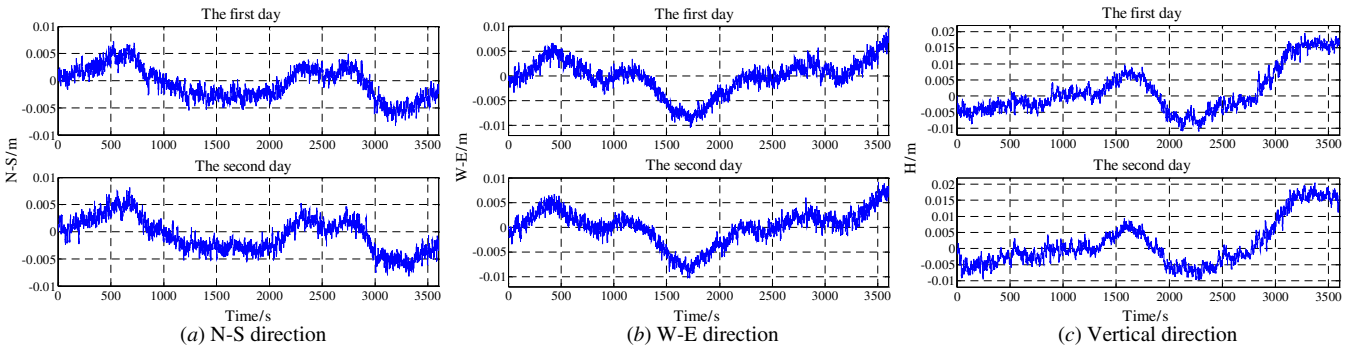

(*a*) N-S direction (*b*) W-E direction (*c*) Vertical direction

Figure 12. Results for two consecutive days in three directions after filtering.

(*a*) 1m (*b*) 4m (*c*) 7m

Figure 13. Set-up of the reflector at different distances of the antenna.

Table 2. Correlation coefficients of two consecutive days before and after filtering.

Direction	N–S	W–E	Height
Before filtering	66.15%	76.37%	76.44%
After filtering	90.60%	93.00%	96.21%

are still differences between them because of the change of uncorrelated noise from day to day.

The filtering is done by the improved particle-filtering algorithm, and systematic resampling is also selected as the resampling algorithm. The filtering results in three directions are shown in figure 12. The correlation coefficients of the two consecutive days before and after filtering are shown in table 2. It is noted from figure 12 and table 2 that the correlations of the consecutively 2 day long data in three directions obviously increase, averagely by 20.28%, and the filtering results are very satisfactory. It indicates that the improved particle-filtering algorithm can effectively remove the receiver's noise and extract the multipath signals caused by the reflective objects in a real environment.

5.4. Characteristics of multipath signal attenuation

In process (4), an experiment using a typical building surface material (ceramic tile) to examine the characteristics of reflection attenuation was conducted, as shown in figure 13. For simulating the reflection propagation, it is assumed that every signal be specularly reflected by a mirror-like surface that reflects a signal from a single incoming direction to a single outgoing direction. A preliminary experiment was first carried out to check for satellite availability. Seven or more satellites were visible at all times during the three days of testing. Also, the positional dilution of precision (PDOP) was below 3 at all times during the testing. The recorded signals of every day were first analyzed to ensure that the rover had not lost the lock during the observation period. Any observations where the lock on the satellite had been lost, were removed from the output. Since the full 24 h sidereal day plot is too long to include here, only an excerpt (1 h) is provided to demonstrate the results.

The results recorded in process (2), when the antenna was unobstructed, were taken as the control. Any deviation from this value, found in process (4), was computed as an error in the results. This error can only be attributed to the presence of a ceramic tile obstructing the transmitting antenna of the rover, since all other variables were kept constant. The computed results are shown in figure 14. Based on the characteristics of the GPS receiver's noise obtained in process (2), the results processed by the improved particle filter are shown in figure 15. From the visual inspection of figure 15, it actually seems that the improved particle-filtering algorithm gives significantly improved results when the reflector is at different distances compared with these data in figure 14. So this algorithm has the advantage of being able to adapt to the close reflector situation, while remaining quite efficient when the reflector gets further away (1, 4 and 7 m during the present tests).

The amplitude and standard deviation of multipath signals as shown in table 3 are obtained from the results of 1, 4 and

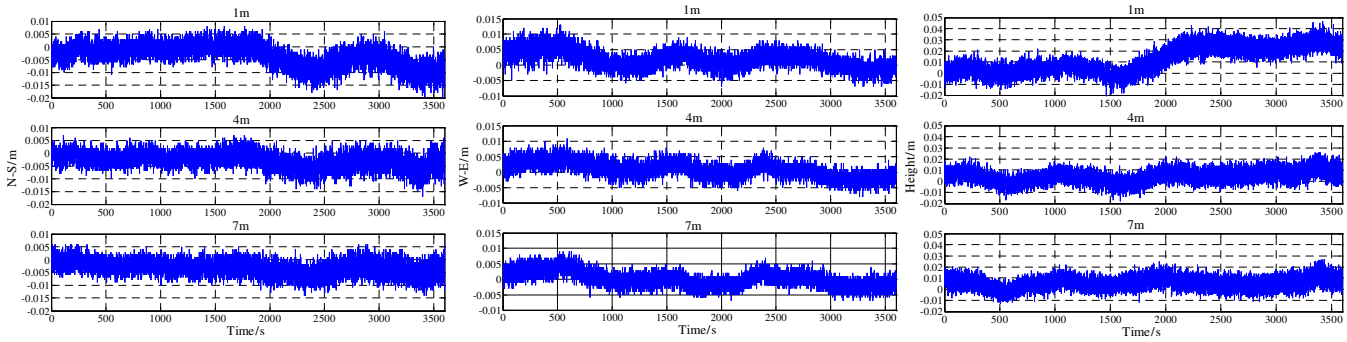

(*a*) N-S direction (*b*) W-E direction (*c*) Vertical direction

Figure 14. Influence of the distance between the rover's antenna and the reflector.

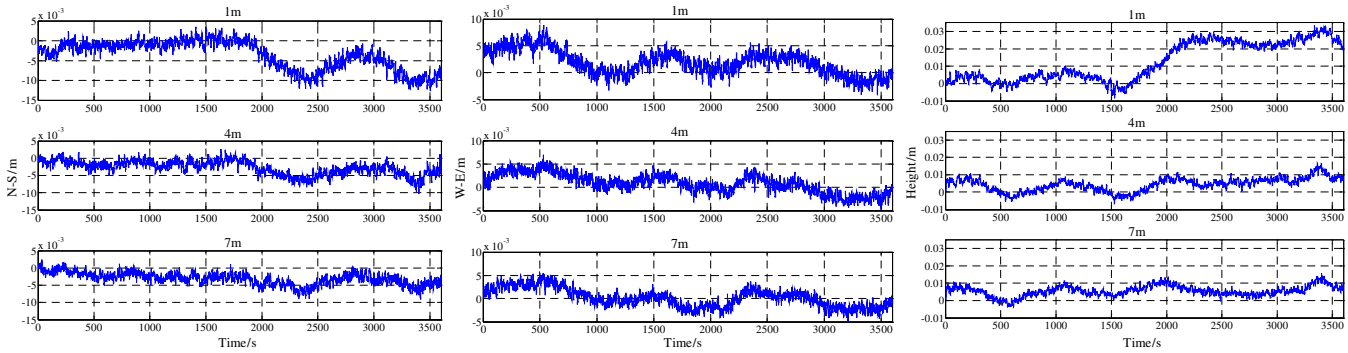

(*a*) N-S direction (*b*) W-E direction (*c*) Vertical direction

Figure 15. Multipath observables corresponding to different distances of the reflector.

Table 3. Amplitude and standard deviation of multipath signals after filtering (unit: cm).

	N–S			W–E			Height		
Parameter	1 m	4 m	7 m	1 m	4 m	7 m	1 m	4 m	7 m
Maximum	0.35	0.24	0.21	0.89	0.70	0.58	3.35	1.68	1.56
Minimum	−1.27	−1.03	−0.91	−0.44	−0.43	−0.43	−0.86	−0.64	−0.44
Standard deviation	0.39	0.36	0.20	0.18	0.23	0.21	0.20	0.89	0.39

Table 4. Correlation coefficients of multipath signals after filtering.

	N–S		W–E		Height	
Parameter	1 and 4 m	1 and 7 m	1 and 4 m	1 and 7 m	1 and 4 m	1 and 7 m
Correlation coefficients	75.55%	60.07%	75.79%	65.17%	68.90%	32.80%

7 m after filtering. From table 3, it can be concluded that the amplitude of multipath signals in three directions decreases with the increase in distances, and the decreased rate gets smaller, while the minimum value in the W–E direction has no obvious change. The changed rate of multipath signals in the vertical direction is about two times that in the plane, and the multipath signals tend to be gentle along with the increase of distances in three directions. The daily repeatability is given by the correlation among those data series as shown in table 4. This suggests the presence of the multipath generated by the ceramic tile. From table 4, it is shown that although there are certain correlations between multipath signals along with the increase in the distance, the correlations gradually become smaller.

6. Conclusions

Despite continuing improvements in the GPS receivers and antennas, the multipath signals still remain as a dominant cause of error. Driving down the multipath signals is probably the single-most important objective of current research into the use of the GPS for highly accurate applications. From the practical point of view, understanding the characteristics of multipath effects on the kinematic GPS techniques is extremely useful. By means of computer simulation, it can be seen that the relative carrier-phase-based GPS precise positioning is subject to a number of error sources, and most of these factors are closely related to the reflecting environment. In static applications, this may be accomplished by averaging over

a sufficiently long period of observation, but in kinematic applications, a modeling approach must be used.

For this reason, this paper focuses on an improved particle-filtering algorithm for multipath extraction, and is especially relevant to applications that require very high accuracy positioning over short and medium distances where the GPS multipath signals exhibit a very high degree of spatial correlation. A controlled multipath environment has been established and fully calibrated for both static and kinematic tests. Experimental results have shown that the algorithm has the advantage of being able to adapt to the close reflector situation, while remaining quite efficient when the reflector gets further away. This equipment could also be used in the future to assess the efficiency of any new multipath mitigation strategy.

The day-to-day repeatability of the multipath can be exploited to improve positioning accuracies. Given known coordinates of a point, the multipath signal at every epoch can be extracted by the improved particle-filtering algorithm from the collected phase data. This multipath signal can then be subtracted from the data collected the subsequent day. Although this procedure increases the noise of the corrected measurements, it removes the multipath almost completely. What needs to be emphasized is that the method is based upon the premise in which the monitoring antennas do not change significantly per day; thus, the multipath effect at each monitoring station will repeat each sidereal day. This is an acceptable assumption in most deformation monitoring situations.

Acknowledgments

This research work was jointly supported by the Program for New Century Excellent Talents in University (grant no NCET-10), the National Natural Science Foundation of China (grant no 50708013), the Special Program (grant no 200902255) of China Postdoctoral Science Foundation, and the Open Fund of State Key Laboratory of Coastal and Offshore Engineering (grant no LP0905).

References

[1] Elsobeiey M and El-Rabbany A 2010 On stochastic modeling of the modernized global positioning system (GPS) L2C signal *Meas. Sci. Technol.* **21** 055105

[2] Kijewski-Correa T and Michael K 2007 Monitoring the wind-induced response of tall buildings: GPS performance and the issue of multipath effects *J. Wind Eng. Ind. Aerodyn.* **95** 1176–98

[3] Peyret F, Betaille D and Hintzy G 2000 High-precision application of GPS in the field of real-time equipment positioning *Autom. Constr.* **9** 299–314

[4] Satirapod C, Khoonphool R and Rizos C 2003 Multipath mitigation of permanent GPS stations using wavelets *Proc. Int. Symp. on GPS/GNSS (Tokyo, Japan, 15–18 November 2003)*

[5] Wang J, Wang J L and Roberts C 2009 Reducing carrier phase errors with EMD-wavelet for precise GPS positioning *Surv. Rev.* **41** 152–61

[6] Axelrad P, Comp C J and MacDoran P F 1994 Use of signal-to-noise ratio for multipath error correction in GPS differential phase measurements: methodology and experimental results *Proc. 7th Int. Technology Meeting of the Satellite Division of the US Institute of Navigation (Salt Lake City, USA, 20–23 September 1994)* pp 655–66

[7] Bétaille D F, Cross P A and Euler H J 2006 Assessment and improvement of the capabilities of a window correlator to model GPS multipath phase errors *IEEE Trans. Aerosp. Electron. Syst.* **42** 705–17

[8] Fan K K and Ding X L 2006 Estimation of GPS carrier phase multipath signals based on site environment *J. Glob. Positioning Syst.* **5** 22–8

[9] Rouabah K and Chikouche D 2009 GPS/Galileo multipath detection and mitigation using closed-form solutions *Math. Probl. Eng.* **2009** 106870

[10] Zhang Z and Law C W 2005 Short-delay multipath mitigation technique based on virtual multipath *IEEE Antennas Wirel. Propag. Lett.* **4** 344–8

[11] Nagano T and Iwamoto T 2009 Multipath estimation of GPS signals and a C-A code conversion technique for efficient computation *Proc. 6th Workshop on Positioning, Navigation and Communication (WPNC'09) (Leibniz, Germany, 19 March 2009)* pp 203–8

[12] Zhang Z, Law C L and Gunawan E 2007 Multipath mitigation technique based on partial autocorrelation function *Wirel. Pers. Commun.* **41** 145–54

[13] Zhang Y H, Yi T H, Li H N and Gu M 2008 Research progress of multipath effect in GPS structural health monitoring *Proc. 2nd Int. Forum on Advances in Structural Engineering (IFASE2008) (Dalian, China, 10–12 October 2008)*

[14] Lee Y W, Suh Y C and Shibasaki R 2008 A simulation system for GNSS multipath mitigation using spatial statistical methods *Comput. Geosci.* **34** 1597–609

[15] Yuan L G, Huang D F, Ding X L, Xiong Y L and Zhong P 2004 On the influence of signal multipath effects in GPS carrier phase surveying *Acta Geod. Cartographica Sin.* **33** 210–5

[16] Aggarwal P, Syed Z and El-Sheimy N 2009 Hybrid extended particle filter (HEPF) for integrated inertial navigation and global positioning systems *Meas. Sci. Technol.* **20** 055203

[17] Doucet A, Godsill S J and Andrieu C 2000 On Monte Carlo sampling methods for Bayesian filtering *Stat. Comput.* **10** 197–208

[18] Gordon N J, Salmond D J and Smith A F M 1993 Novel approach to nonlinear/non-Gaussian Bayesian state estimation *IEEE Proc. Radar Signal Process.* **140** 107–13

[19] Hol J, Schon T B and Gustafsson F 2006 On resampling algorithms for particle filters *Proc. Nonlinear Statistical Signal Processing Workshop (Cambridge, UK, 13–15 September 2006)* pp 79–82

[20] Douc R, Cappe O, Polytech E and Palaiseau F 2005 Comparison of resampling schemes for particle filtering *Proc. 4th Int. Symp. on Image and Signal Processing and Analysis (ISPA) (Zagreb, Croatia, 15–17 September 2005)* pp 64–9